IEEE Open Journal of Vehicular Technology

Received 27 March 2024; accepted 14 April 2024. Date of publication 17 April 2024;
date of current version 1 May 2024. The review of this article was coordinated by Editor Shuaishuai Guo.

Digital Object Identifier 10.1109/OJVT.2024.3390204

Receiver Design for OFDM Schemes With Low-Resolution ADCs

JOÃO MADEIRA [1,2], ZAHRA MOKHTARI [1] (Member, IEEE), JOÃO GUERREIRO [1,2] (Senior Member, IEEE), AND RUI DINIS [1,2] (Senior Member, IEEE)

[1]IT, Instituto de Telecomunicações, 3810-193 Aveiro, Portugal
[2]FCT, Universidade NOVA de Lisboa,1099-085 Lisboa, Portugal

CORRESPONDING AUTHOR: JOÃO MADEIRA (e-mail: jf.madeira@campus.fct.unl.pt).

This work was supported in part by the Lund Research Center, Huawei Technologies Sweden AB, Sweden, in part by the FCT - Fundação para a Ciência e Tecnologia and Instituto de Telecomunicações under Ph.D. Grant UI/BD/150877/2021 doi: 10.54499/UI/BD/150877/2021, in part by Project under Grant UIDB/50008/2020, and in part by Project CELL-LESS6G under Grant 2022.08786.PTDC.

ABSTRACT Is is widely known that the power consumption of Analog-to-Digital Converters (ADCs) is strongly related with the number of bits of resolution. Using smaller resolutions can greatly reduce the power consumption of the RX frontend. However, the use of low-resolution ADCs introduces significant nonlinear distortion, especially when Orthogonal Frequency Division Multiplexing (OFDM) signals are employed, which might severely degrade performance. In this work, we consider nonlinear effects at the receiver side, associated with quantization and saturation of low-resolution ADCs, and we propose a Generalized Approximate Message Passing (GAMP) receiver that is specially designed to cope with nonlinear effects at the OFDM receiver. We show that our receiver can significantly mitigate the distortion that arises from low-resolution ADCs, allowing larger M-ary Quadrature Amplitude Modulation (M-QAM) constellations to be employed. The proposed receiver is shown to be robust to strong channel fading effects, as well as errors during the channel estimation process.

INDEX TERMS OFDM, GAMP, ADC, nonlinear effects.

I. INTRODUCTION

The ubiquity of wireless devices has motivated the development of faster and more reliable connections. To achieve this kind of performance, linear transceivers should be deployed, namely using higher-quality hardware, such as high-resolution Digital-to-Analog Converters (DAC) at the transmitter and Analog-to-Digital Converters (ADC) at the receiver. As is widely known, using data converters with high resolution results in lower signal distortion levels, and, consequently, improved performance, especially when higher-order modulations are employed, which are more sensitive to noise and residual interference. However, higher resolutions increase device complexity and power consumption [1]. In fact, the power consumption of an ADC can be exponentially proportional to the bit resolution [2].

The alternative of using low-resolution converters introduces nonlinear distortion on the signal which negatively impacts the systems's performance. Generally, in selecting the DAC/ADC resolution there is a trade-off between distortion and hardware savings [3]. If the system can cope with this distortion, then it can enable lower resolution and decrease power consumption and cost at the DAC/ADC. There are many schemes to cope with the nonlinear distortion due to the DAC, such as the use of multiple antennas at the transmitter side can reduce the performance degradation associated with the use of low-resolution DACs [4], it can also lead to spectral regrowth outside of the signal bandwidth that may be incompatible with Spectral Emission Masks (SEM). For the receiver side, the spectral widening associated with low-resolution ADCs does not lead to spectral regrowth, so it is reasonable to expect scenarios where ADCs have lower resolution than DACs employed at the transmitter. Naturally, this leads to higher distortion at the detection level, which increases if the oversampling factor is not large enough to mitigate the aliasing effects. Another key aspect is the ADC input range, or saturation, which defines the range of

© 2024 The Authors. This work is licensed under a Creative Commons Attribution-NonCommercial-NoDerivatives 4.0 License. For more information, see https://creativecommons.org/licenses/by-nc-nd/4.0/

acceptable input signals that will be converted to a digital code. If an input signal falls outside of this range, it will be clipped to the maximum or minimum code. The input signal range is defined by the Automatic Gain Control (AGC) of the receiver, which in practice does not have an ideal response [5].

Several techniques have been proposed to cope with nonlinear distortion effects. The most common take advantage of Bussgang's theorem [6] to decompose the received signal into useful and distortion components and estimate and cancel the latter using an iterative process [7]. A more powerful technique is the Generalized Approximate Message Passing (GAMP) receiver [8], which is a low complexity approximation of Bayesian inference for linear observations. In the literature, GAMP has been proposed as a suboptimum receiver for nonlinearly distorted observations [9]. In these scenarios it has been shown to achieve excellent performance, even surpassing conventional systems without nonlinear distortion [10], [11]. This surprising result was also observed in the modified GAMP receiver proposed in [12], which also presents less complexity than conventional GAMP. These implementations only consider nonlinearities at the transmitter and assume ideal receiver hardware, such as infinite-resolution ADCs. Although, due to data processing inequality, it is impossible to increase channel capacity via post-processing at the receiver [13], we can design a receiver that takes into account the nonlinear function applied to the signal to minimize the impact on performance. A GAMP-based approach was proposed in [14], though it did not consider the nonlinear distortion due to low ADC saturation. In [15], the authors consider an Approximate Message Passing (AMP) received to cope with low-resolution ADCs, though it does not benefit from knowing the nonlinear function. The authors of [16] propose an iterative Generalized Turbo (GTurbo) technique that can perform detection and channel estimation, at the cost of high complexity. [17] presents a linear precoding scheme that takes advantage of antenna diversity to cope with 1-bit resolution DACs, but it requires additional antennas. A deep learning approach for detection and channel estimation using 1-bit ADCs is proposed in [18], although it requires supervised learning and even higher complexity in the unsupervised case. A GAMP-based receiver for Line-of-Sight (LoS) scenarios that outperforms conventional Bussgang receivers was proposed in [19], though the authors did not consider large constellations.

In this work, we consider a scenario where the receiver employs a low-resolution ADC. This enables a significant reduction in device cost and power consumption, at the cost of increased nonlinear distortion. To cope with this distortion, the receiver employs a GAMP-based iterative algorithm that attempts to minimize the impact of the nonlinearity. By separating the in-phase (I) and quadrature (Q) branches' processing, we demonstrate that the complexity of GAMP can be substantially reduced, compared to previous works [10], while still being able to outperform conventional receivers that use low-resolution ADCs. In fact, GAMP even performs better when low ADC saturation is considered, because the quantization noise is lower. This highlights the nonlinear distortion reobustness of GAMP over conventional receivers. In scenarios with frequency-selective channels, the proposed receiver is modified to include channel coding, which drastically improves performance, even for very low ADC resolutions.

The paper is organized as follows: Section. II characterises the wireless transceiver setup; Section. III details the GAMP algorithm structure; Section. IV characterizes the frequency-selective channel scenario; Section. V defines the proposed coded GAMP receiver; Section. VI presents simulation results of the proposed system; Section. VII concludes this paper.

In this work we utilize the following notation. A vector is denoted in bold as $\mathbf{X}$, with a single element written with a subscript index denoting the position in the vector as X_n. For matrices, we utilize multiple subscripts, such as $X_{n,k}$, to denote an entry in a 2-D matrix. We use $\mathcal{R}$ and $\mathcal{I}$ to denote the real and imaginary parts of a complex-valued number, respectively. We use $\mathcal{N}(\mu, 2\sigma^2)$ to denote a complex Normal distribution with mean μ and variance $2\sigma^2$.

II. SYSTEM CHARACTERIZATION

We consider an Orthogonal Frequency Division Multiplexing (OFDM) downlink communication employing M-ary Quadrature Amplitude Modulation (M-QAM). The transmitted signal is defined in the frequency domain as the vector of complex-valued data symbols

$$\mathbf{X} = [X_0, X_1, \ldots X_{N-1}], \tag{1}$$

where N is the number of subcarriers. We can express the received signal at the kth subcarrier as

$$Y_k = X_k + N_k, \tag{2}$$

where N_k is the complex Additive White Gaussian Noise (AWGN) associated with the kth subcarrier with distribution $\mathcal{N}(0, 2\sigma_N^2)$. Before detection, the received signal is converted to the digital domain using an ADC with limited resolution and a given saturation level. We represent this quantization process as a memoryless nonlinear function $f(\cdot)$ that is applied to the time domain counterpart of Y_k, written as y_n. The corresponding nonlinearly distorted signal associated with the nth time domain sample is defined as

$$y_n^{nl} = f\left(\mathcal{R}\left(y_n\right)\right) + jf\left(\mathcal{I}\left(y_n\right)\right), \tag{3}$$

with a frequency domain counterpart Y_k^{nl}, defined as

$$Y_k^{nl} = \sum_{n=0}^{N-1} F_{n,k} y_n^{nl}, \tag{4}$$

where $\mathbf{F}$ is the Discrete Fourier Transform (DFT) matrix of order N. The matrix multiplication is computed using a Fast Fourier Transform (FFT). The branch function of the ADC, $f(\cdot)$, is defined as [20]

$$f(x) = \text{round}\left(\frac{x}{2^{R_{bit}-1}}\right) A_{bit}, \tag{5}$$

where the function round$(\cdot)$ rounds the operand to the nearest integer, R_{bit} is the ADC bit resolution, and A_{bit} is the Least

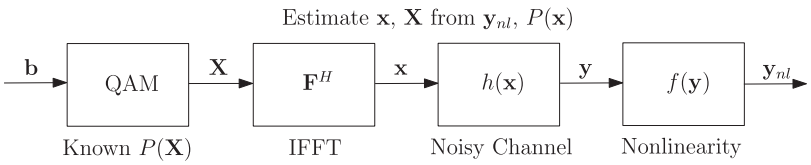

FIGURE 1. Diagram of the general nonlinear model for noisy nonlinear estimation.

Significant Bit (LSB) amplitude, which depends on the ADC saturation amplitude A_{sat}, and is defined as

$$A_{bit} = \frac{A_{sat}}{2^{R_{bit}-1}}. \tag{6}$$

The ADC is applied independently to the in-phase and quadrature components, using the same R_{bit} and A_{bit} for both. After digital conversion, data detection is performed on the frequency-domain signal Y_k^{nl}.

III. GAMP RECEIVER

As aforementioned, using low-resolution ADCs can lead to significant savings in the RX radio frontend. According to [2], the power consumption of an ADC is proportional to $2^{R_{bit}}$. Therefore, each reduction in bit resolution, halves the consumed power of the ADC. For low-resolution ADCs, the nonlinear distortion effects can be very high. By assuming that all input values are within the ADC range, the average power of the distortion can be approximated as $\frac{A_{bit}^2}{12}$ [21]. Therefore, recovering the original linear signal is difficult due to the presence of this distortion, which cannot be decoupled due to the nonlinear nature of $f(\cdot)$. Therefore, a conventional receiver will only successfully perform detection if the quantization noise and nonlinear distortion due to saturation are sufficiently low. In this sense, it is useful to characterize this problem as a modification to the Generalized Linear Model (GLM), where an additional nonlinear function is applied to the signal after the noisy channel, resulting in a nonlinearly distorted estimate, as shown in Fig. 1.

An interesting approach that has come up in recent literature is the GAMP algorithm, which consists of an iterative detection scheme that can perform near-optimum detection of nonlinearly distorted signals. Although most implementations consider a nonlinearity at the transmitter, since it is the optimum configuration [22], GAMP can also be used to improve detection in scenarios where the nonlinearity is at the receiver [14]. Although GAMP introduces significant complexity in receiver design, it allows for substantial savings in the ADC. The proposed GAMP decoder, based on [10], is shown in Algorithm 1.

For better performance, received signals can be oversampled by a factor O_s before the GAMP receiver. Higher oversampling ratios have been adopted in previous works [23] since they allow for faster and more stable convergence by reducing the aliasing associated with the Out-of-Band (OOB) radiation. In addition, oversampling by a factor of $O_s = 4$ is equivalent to increasing the ADC resolution by 1-bit [24], which further improves performance. In this case, the DFT matrix $\mathbf{F}$ is of order NO_s. From this point on, the iteration indices from GAMP variables are omitted to simplify the notation. For MMSE estimation, the input nonlinear function g_{in} and its derivative g'_{in} are defined as [8]

$$g_{in}\left(\hat{V}_k, \mu^V\right) := \mathrm{E}\left[X_k|\hat{V}_k\right] \tag{7}$$

Algorithm 1: GAMP Receiver.

Given a nonlinearly distorted received signal in the time domain, $\mathbf{y}^{nl}$, produce an estimate, $\hat{\mathbf{X}}$, of the original transmitted data $\mathbf{X}$.

1) Initialization

$$i = 1, \hat{\mathbf{X}}(1) = \mathbf{0}_{NO_s,1}, \hat{\mathbf{s}}(0) = \mathbf{0}_{NO_s,1}, \mu^X(1) = \mathbf{1}_{NO_s,1}$$

2) Output linear step

$$\mu^p(i) = \frac{1}{NO_s}\sum_{k=0}^{NO_s-1}\mu_k^X(i)$$

$$\hat{p}_n(i) = \sum_{k=0}^{NO_s-1}\left(F_{n,k}^H\hat{X}_k(i)\right) - \mu^p(i)\hat{s}_n(i-1), \forall n$$

3) Output nonlinear step

$$\hat{s}_n(i) = (1-\beta)\,\hat{s}_n(i-1) + \beta g_{out}(\hat{p}_n(i), \mu^p(i), y_n^{nl}), \forall n$$

$$\mu_n^s(i) = (1-\beta)\,\mu_n^s(i-1) - \beta\frac{\partial}{\partial\hat{p}_n}g_{out}(\hat{p}_n(i), \mu^p(i), y_n^{nl}), \forall n$$

4) Input linear step

$$\tilde{X}_k(i) = (1-\beta)\tilde{X}_k(i-1) + \beta\hat{X}_k(i), \forall k$$

$$\mu^V(i) = \left(\frac{1}{NO_s}\sum_{n=0}^{NO_s-1}\mu_n^s(i)\right)^{-1}, \forall k$$

$$V_k(i) = \tilde{X}_k(i) + \mu_k^V(i)\sum_{n=0}^{NO_s-1}F_{n,k}\hat{s}_n(i), \forall k$$

5) Input nonlinear step

$$\hat{X}_k(i+1) = g_{in}\left(\hat{V}_k(i), \mu_k^V(i)\right), \forall k$$

$$\mu_k^X(i+1) = -\mu_k^V(i)\frac{\partial}{\partial\hat{V}_k}g_{in}\left(\hat{V}_k(i), \mu_k^V(i)\right), \forall k$$

and

$$-\mu^V \frac{\partial}{\partial \hat{V}_k} g_{in} := \text{var}\left[X_k|\hat{V}_k\right]. \tag{8}$$

The expectation for M-QAM can be calculated by [9]

$$\text{E}\left[X_k|\hat{V}_k\right] = \sum_{i=0}^{M-1} D_i P\left(D_i|\hat{V}_k, \mu^V\right), \tag{9}$$

where D_i is the ith symbol of the constellation, and $P(D_i|\hat{V}_k\mu^V)$ is the likelihood of that symbol, defined as

$$P\left(D_i|\hat{V}_k, \mu^V\right) = \frac{\exp\left(-\frac{|D_i-\hat{V}_k|^2}{2\mu^V}\right)}{\sum_{j=0}^{M-1}\exp\left(-\frac{|D_j-\hat{V}_k|^2}{2\mu^V}\right)}. \tag{10}$$

The variance of the distribution is calculated as

$$\text{var}\left[X_k|\hat{V}_k\right] = \sum_{i=0}^{M-1}\left(D_i - \text{E}\left[X_k|\hat{V}_k\right]\right)^2 P\left(D_i|\hat{V}_k, \mu^V\right). \tag{11}$$

For $O_s > 1$, which is usually the case, the unused subcarriers are set as $\hat{X}_k = 0$ and $\mu_k^X = 1$, for $O_sN > k > N$. The output nonlinear function g_{out} for MMSE estimation is defined as [8]

$$g_{out}\left(\hat{p}_n, \mu^p, y_n^{nl}\right) = \frac{\hat{s}_0 - \hat{p}_n}{\mu^p}, s_0 := \text{E}\left[s|\hat{p}_n, y_n^{nl}, \mu^p\right]. \tag{12}$$

In the scenario considered in this work, the observation vector was submitted to a nonlinear function. As was shown in the results of [10], taking into account the nonlinear distortion in the likelihood calculations yields better performance, hence this work makes use of the nonlinear function of the ADC in the likelihood estimations. In the general case, the expectation can only be computed through complex numerical integration, as proposed in [9]. This requires a large number of operations that is quadratically proportional to the number of integration points. However, since the ADC nonlinearity is applied separately to the in-phase and quadrature components, referred to as a rectangular nonlinearity, then it is possible to divide the complex-valued double integral into two real-valued, single integrals. The real component is calculated as

$$\mathcal{R}(\text{E}[s|\hat{p}_n, y_n^{nl}, \mu^p]) = \frac{1}{C^R}\int_{-\infty}^{\infty} x e^{-\frac{|\mathcal{R}(y_n^{nl})-f(x)|^2}{2\sigma_N^2} - \frac{|\mathcal{R}(\hat{p}_n)-x|^2}{2\mu_p}} \text{d}x, \tag{13}$$

and the imaginary component as

$$\mathcal{I}(\text{E}[s|\hat{p}_n, y_n^{nl}, \mu^p]) = \frac{1}{C^I}\int_{-\infty}^{\infty} xje^{-\frac{|\mathcal{I}(y_n^{nl})-f(x)|^2}{2\sigma_N^2} - \frac{|\mathcal{I}(\hat{p}_n)-x|^2}{2\mu_p}} \text{d}x, \tag{14}$$

where C^R and C^I are normalization constants defined as

$$C^R = \int_{-\infty}^{\infty} e^{-\frac{|\mathcal{R}(y_n^{nl})-f(x)|^2}{2\sigma_N^2} - \frac{|\mathcal{R}(\hat{p}_n)-x|^2}{2\mu_p}} \text{d}x, \tag{15}$$

and

$$C^I = \int_{-\infty}^{\infty} e^{-\frac{|\mathcal{I}(y_n^{nl})-f(x)|^2}{2\sigma_N^2} - \frac{|\mathcal{I}(\hat{p}_n)-x|^2}{2\mu_p}} \text{d}x. \tag{16}$$

The integration variable is defined to be between $[-A_x, A_x]$, with N_x points in between, for a total $2N_x$ operations, which is a substantial reduction from complex integration with N_x^2 operations. The partial derivative of g_{out} is defined as

$$\frac{\partial}{\partial \hat{p}_n} g_{out}\left(\hat{p}_n, \mu_n^p, y_n^{nl}\right) = \frac{1}{\mu^p}\left(1 - \frac{\text{var}\left[s|\hat{p}_n, y_n^{nl}, \mu^p\right]}{\mu^p}\right), \tag{17}$$

where $\text{var}[s|\hat{p}_n, y_n^{nl}, \mu^p]$ can be calculated as the sum of two real-valued integrals, calculated as

$$\text{var}[s|\hat{p}_n, y_n^{nl}, \mu^p] = \frac{1}{C^R}\int_{-\infty}^{\infty}|x|^2 e^{-\frac{|\mathcal{R}(y_n^{nl})-f(x)|^2}{2\sigma_N^2} - \frac{|\mathcal{R}(\hat{p}_n)-x|^2}{2\mu_p}} \text{d}x + \frac{1}{C^I}\int_{-\infty}^{\infty}|x|^2 e^{-\frac{|\mathcal{I}(y_n^{nl})-f(x)|^2}{2\sigma_N^2} - \frac{|\mathcal{I}(\hat{p}_n)-x|^2}{2\mu_p}} \text{d}x - \text{E}[z|\hat{p}, y_n^{nl}, \mu^p]. \tag{18}$$

The GAMP algorithm does not define any stop criteria. Instead, an appropriate method of determining when to stop the algorithm must be developed. The simplest criterion is to stop after $I_{\max}$ iterations, which limits the maximum computation time. However, the proposed GAMP implementation is not guaranteed to converge to the optimum solution, which means that the last iteration may not provide the best estimate of X_k in terms Bit Error Rate (BER) performance.

In this work, we consider a scenario wherein the data contains a Cyclic Redundancy Check (CRC) code powerful enough to detect a significant amount of errors in the data. After each iteration, the CRC is checked and the amount of errors is computed. If there are no errors, then the algorithm terminates, else it continues to the next iteration. If $I_{\max}$ iterations are reached, then the iteration with the least amount of bit errors is selected as the best. For simplicity, we do not consider the impact of the CRC code on the spectral efficiency.

IV. GAMP RECEIVER FOR FREQUENCY-SELECTIVE CHANNELS

In this section, we will analyze the implications of fading in the wireless channel. In this scenario, the receiver requires Channel State Information (CSI) to perform detection. The channel frequency response for a given OFDM symbol is defined as

$$\mathbf{H} = \left[H_0, H_1, \ldots, H_{N-1}\right], \tag{19}$$

where H_k refers to the complex coefficient associated with the kth subcarrier. If the Cyclic Prefix (CP) is longer than the Channel Impulse Response (CIR) length, then the received signal can be defined in the frequency domain as

$$Y_k = X_k H_k + N_k. \tag{20}$$

This allows the use of simple, single-tap equalizers such as the Zero Forcing (ZF) equalizer to invert the channel effects. With ZF, the equalized signal is given by

$$\tilde{X}_k = \frac{Y_k^{nl}}{H_k}. \tag{21}$$

Although there can be numerical issues in ZF if $H_k \to 0$, we will show that this problem can be mitigated by using soft decisions. In general, obtaining CSI at the receiver can be difficult when low-resolution ADCs take place. However, it has been shown that GAMP-based approaches can achieve excellent performance even when only imperfect CSI is available [27], [28]. A deep learning-based receiver [29] was also compared favorably to GAMP techniques for channel estimation. In this work, we are concerned with the impact on data detection, and as such will consider, without loss of generality, that the CSI is obtained prior to GAMP decoding.

Due to the multi-carrier nature of OFDM, subcarriers affected by strong fading may result in lost information bits. For this reason, Forward Error Correction (FEC) is always used with OFDM in frequency-selective channels. In current high data rate standards for wireless communication, FEC is implemented via turbo convolutional Codes, polar codes, and Low-Density Parity Check (LDPC) codes [25]. Although each code differs in implementation, structure, and error-correcting capabilities, we will limit our analysis to LDPC codes, which can be trivially extended for other types of codes.

The encoding process of an LDPC code is where most of the computational complexity associated with the code lies, and can be reduced by using appropriate parity matrices. As an example, the parity matrix, $\mathbf{H_P}$ from [26], which is comprised of $N_P = 2016$ and $K_P = 1008$ variable and parity check nodes, respectively, with a code rate $R = 1/2$. Decoding is performed using the well-known Soft-Input, Soft-Output (SISO) Belief Propagation (BP) decoder, which takes as inputs the bit-wise reliabilities, as opposed to the decided bits, which can be expressed as the Log-Likelihood Ratio (LLR) for each bit. The LLR of the mth bit is defined as

$$\begin{aligned} L_m \approx \frac{|H_k|^2}{2\sigma_N^2} &\left(\mathcal{R}\left(\tilde{X}_k - X_k^1\right) + \mathcal{I}\left(\tilde{X}_k - X_k^1\right)\right. \\ &\left. -\mathcal{R}\left(\tilde{X}_k - X_k^0\right) - \mathcal{I}\left(\tilde{X}_k - X_k^0\right)\right), \end{aligned} \tag{22}$$

where X_k^1 and X_k^0 are the closest symbols to $\tilde{X}_k$, where bit m is equal to 1 and 0, respectively. Since we multiply each LLR by $|H_k|^2$, if $H_k \to 0$, then $\mathbf{L}_k \to 0$, which means the bits associated with the kth subcarrier cannot be correctly detected.

Additionally, the LDPC SISO decoder also outputs an updated vector of LLRs corresponding to the original codeword. This optional output requires no additional complexity, as it is a byproduct of BP decoding, and can be used in iterative receivers, such as the Bussgang receiver, to improve the quality of the estimate used in the next iteration.

A. IMPERFECT CSI

The detection performance of the receiver is strongly dependent on the accuracy of the CSI. We consider that the receiver may not have perfect CSI, with the channel matrix available at the receiver being defined as

$$\hat{H}_k = \rho H_k + \epsilon_k, \tag{23}$$

where $\rho \in [0, 1]$ is a correlation factor with the ideal channel, and ϵ_k is an error term that follows a Gaussian distribution $\mathcal{N}(0, 1 - \rho^2)$. This model was shown to be accurate for modeling channel estimation errors in the receiver [30]. For convenience, we express the error variance in decibel (dB), defined as

$$\sigma_E = 10 \log_{10}\left(1 - \rho^2\right). \tag{24}$$

When imperfect CSI is considered, the receiver utilizes $\hat{H}_k$, as opposed to H_k in the calculations.

V. CODED GAMP

To handle frequency-selective channels, we modify the previous algorithm to take into account the CSI. This modified GAMP behavior is described in Algorithm. 2. This modification includes incorporating $\mathbf{H}$ as part of the linear transformation matrix, which can only be done due to the nonlinearity being present at the receiver, unlike [9], [10] where the nonlinearity is at the transmitter. Although this process introduces additional complexity due to channel multiplication, it should be noted that other iterative receivers, such as Bussgang receivers, may also require multiple channel inversions to perform the data detection, depending on the equalization scheme.

At the end of step 4, the SISO decoder is executed using the bit LLRs, which are computed as

$$\begin{aligned} L_m^{(i)} \approx \frac{1}{2\mu_k^V} &\left(\mathcal{R}\left(\hat{V}_k - V_k^1\right) + \mathcal{I}\left(\hat{V}_k - V_k^1\right)\right. \\ &\left. -\mathcal{R}\left(\hat{V}_k - V_k^0\right) + \mathcal{I}\left(\hat{V}_n - V_k^0\right)\right), \end{aligned} \tag{25}$$

where V_k^1 and V_k^0 are the closest symbols to $\hat{V}_k$, where bit m is equal to 1 and 0, respectively. In this fashion, the decoding step can also be used as an early stop condition for GAMP, when all parity checks are met. For this application, the high error-detecting capability of LDPC codes is extremely useful.

As is the case for the Bussgang receiver, GAMP can also take advantage of the optional coded output of the SISO decoder to improve convergence speed. This requires rewriting the a priori symbol probabilities $P(D_i|\hat{V}_k, \mu^V)$ as [31]

$$P(D_i|\hat{V}_k, \mu_k^V) = \prod_{j=0}^{\log_2(M)-1} \frac{1}{2}\left(1 + \tilde{b}_{k,j} \tanh \frac{L_{k,j}^c}{2}\right), \tag{26}$$

where L_j^C is the coded output of the SISO decoder for the jth bit of the kth symbol, and $\tilde{b}_{k,j}$ is defined as

$$\tilde{b}_{k,j} := \begin{cases} 1, & b_{k,j} = 0 \\ -1, & b_{k,j} = 1 \end{cases}, \tag{27}$$

Algorithm 2: Coded-GAMP Receiver.

Given a nonlinearly distorted received signal in the time domain, $\mathbf{y}^{nl}$, and CSI $\mathbf{H}$, produce an estimate, $\hat{\mathbf{X}}$, of the original transmitted data $\mathbf{X}$.

1) Initialization

$$i = 1, \hat{\mathbf{X}}(1) = \mathbf{0}_{NO_s,1}, \hat{\mathbf{s}}(0) = \mathbf{0}_{NO_s,1}, \mu^X(1) = \mathbf{1}_{NO_s,1}$$

2) Output linear step

$$\mu^p(i) = \frac{1}{NO_s} \sum_{k=0}^{NO_s-1} \mu_k^X(i)$$

$$\hat{p}(i) = \sum_{k=0}^{NO_s-1} \left(F_{n,k}^H H_k \hat{X}_k(i)\right) - \mu^p(i)\hat{s}_n(i-1), \forall n$$

3) Output nonlinear step

$$\hat{s}_n(i) = (1-\beta)\,\hat{s}_n(i-1) + \beta g_{out}(\hat{p}_n(i), \mu^p(i), y_n^{nl}), \forall n$$

$$\mu_n^s(i) = (1-\beta)\,\mu_n^s(i-1) - \beta \frac{\partial}{\partial \hat{p}_n} g_{out}(\hat{p}_n(i), \mu^p(i), y_n^{nl}), \forall n$$

4) Input linear step

$$\tilde{X}_k(i) = (1-\beta)\tilde{X}_k(i-1) + \beta \hat{X}_k(i), \forall k$$

$$\mu_k^V(i) = \left(\frac{|H_k|^2}{NO_s} \sum_{n=0}^{NO_s-1} \mu_n^s(i)\right)^{-1}, \forall k$$

$$V_k(i) = \tilde{X}_k(i) + \mu_k^V(i) H_k^* \sum_{n=0}^{NO_s-1} F_{n,k}\hat{s}_n(i), \forall k$$

5) Input nonlinear step

$$\hat{X}_k(i+1) = g_{in}\left(\hat{V}_k(i), \mu_k^V(i)\right), \forall k$$

$$\mu_k^X(i+1) = -\mu_k^V(i) \frac{\partial}{\partial \hat{V}_k} g_{in}\left(\hat{V}_k(i), \mu_k^V(i)\right), \forall k$$

where $b_{k,j}$ is the jth bit of the kth symbol. In this calculation, μ_k^V is implicit in the previous LLR calculations.

A. COMPLEXITY ANALYSIS

The complexity of GAMP can be characterized per iteration, with total complexity depending on the expected number of iterations. For simplicity, we consider that an arithmetic operation between two real variables consumes 1 flop, with complex variables requiring 2 flops. We can divide an iteration into 4 steps, as was previously shown, numbered between 2 and 5, since step 1 is the initialization.

Step 2 requires computing an average of real numbers, which costs NO_s flops, performing an IFFT of length NO_s, with complexity depending on the architecture, multiplying the channel matrix, and a complex vector-wise multiplication and subtraction, which costs an additional $5NO_s$ flops. The total for this step is $8NO_s$ flops.

Step 3 requires several computations. In [9], [10], the total complexity for this step is $NO_s(3 + 18N_x + 3N_x^2)$. In this work, we considered a rectangular nonlinearity, which allows for a reduction of complexity in this step. The normalization in (15) requires NO_sN_x for the integration, and $6N_x$ flops to calculate the exponent. The exponential is usually sourced from a stored Lookup Table (LUT) and requires no flops [33]. Taking into account (16), this step requires $2NO_s(8N_x)$ flops. The expectations (13) and (14) require $2NO_s(2 + 2N_x)$ flops in total. The nonlinear output step (12) requires the same number of flops. The variance (18) requires $NO_s(3 + 4N_x)$. The total number of flops in this step is $NO_s(5 + 24N_x)$.

Step 4 is similar to step 2, with an additional damping calculation that consumes $6NO_s$ flops. The average requires $1 + NO_s$, due to the mean and negative fraction, and multiplying by the conjugate channel matrix requires NO_s flops. The updated probability requires an FFT of size NO_s and an additional $5NO_s$ flops. The total for this step is $1 + 13NO_s$ flops.

In step 5, the complexity of calculating the likelihood depends on which definition is used. For (10), it requires computing M exponents, each requiring 6 operations and a sum of M complex terms in the denominator. The total is $8M$, assuming that the exponential requires no flops. The expectation in (9) requires $N(12M - 2)$ flops since subcarriers beyond N do not carry data, and the variance (11) requires $N(16M - 2)$, where M is the constellation size. In total, this step requires $N(28M - 4)$ flops.

For coded GAMP, step 5 requires calculating the approximate LLRs for each bit. This consumes $6N\log_2(M)$ flops. Calculating the likelihoods in (26) requires a tanh, which can be sourced from an internal LUT at no flop cost, and an additional $4N\log_2(M)$ flops. The decoding complexity will depend on the chosen decoder structure.

Table 1 summarises the complexity of each GAMP iteration.

From this analysis it is clear how certain variables define the computational complexity of each GAMP step. In step 3 it is clear how the proposed IQ GAMP can achieve a much lower complexity than previous works, as it scales with NO_sN_x, as opposed to $NO_sN_x^2$, allowing for much faster numerical

TABLE 1. Summary of the Complexity in Each Step of GAMP, per Iteration

GAMP Step	Complexity (flops)
Step 2	IFFT+$8NO_s$
Step 3 [9], [10]	$NO_s(3 + 18N_x + 3N_x^2)$
Step 3 IQ	$NO_s(5 + 24N_x)$
Step 4	FFT+$1 + 13NO_s$
Step 5	$N(28M - 4)$
Step 5 Coded	Decoding+$10N\log_2(M)$
Total GAMP	$1 + NO_s(26 + 24N_x) + N(28M - 4)$
Total Coded GAMP	$1 + NO_s(26 + 24N_x) + 10N\log_2(M)$

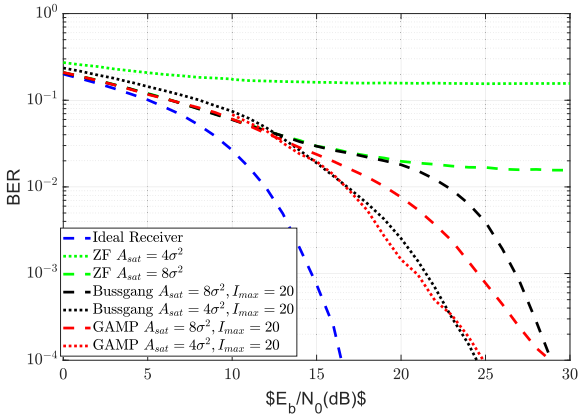

FIGURE 2. BER as a function of the E_b/N_0 for 64-QAM OFDM system with $R_{bit} = 3$, compared with a conventional ZF, Bussgang receiver, and GAMP with $N_x = 256$.

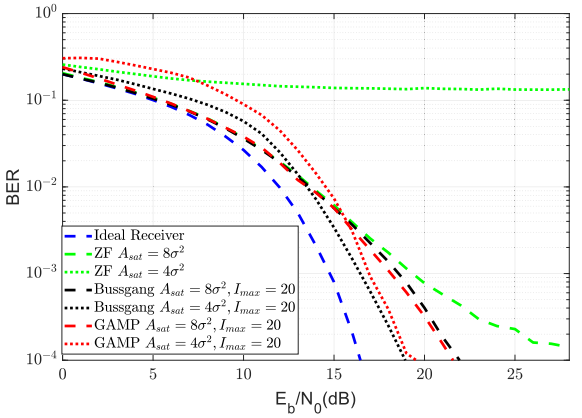

FIGURE 3. BER as a function of the E_b/N_0, for 64-QAM with $R_{bit} = 4$, compared with a conventional ZF, Bussgang receiver, and GAMP with $N_x = 256$.

integration. The term M in step 5 should also be noted, as for very large constellations it may exceed the complexity of step 3, if NO_s is low enough. In coded scenarios, the complexity of this step is lower due to using approximate LLRs, discounting the decoding complexity. The complexity of the other steps is dominated by the DFT, which is implementation-dependent.

Since each iteration decodes the codeword, the per iteration complexity of GAMP is increased by the decoding complexity. Performing $I_{\max}$ GAMP iterations will require $I_{\max}$ times more decoding operations. In the case of LDPC codes, most of the complexity lies in the encoding phase.

VI. PERFORMANCE RESULTS

In this section, we present the performance evaluation of the proposed receiver through a set of Monte Carlo simulations. We consider a transmitter with an ideal DAC that does not introduce distortion in the transmitted signal. Unless specified otherwise, the results were averaged over 1000 OFDM symbol realizations.

A. AWGN CHANNELS

In this subsection, we present the BER performance results of the proposed GAMP receiver considering ideal AWGN channel. The BER is presented as a function of E_b/N_0, which is the ratio between the average bit energy and noise power density. The GAMP's performance is compared with an ideal receiver with infinite precision and no saturation effects, a conventional ZF equalization scheme with a non-ideal ADC, and a Bussgang noise canceling receiver [32] using $I_{\max}$ iterations. It is considered that all receivers operate with the same oversampling factor. The GAMP damping factor was set to $\beta = 0.7$ to improve convergence at the cost of more iterations, while N_x was set at 256 for 64-QAM, and 512 for 256-QAM. We consider ADCs with two values of A_{sat} and different resolutions. The A_{sat} values were selected to assure the lower distortion level for a given ADC resolution.

Fig. 2 presents the BER performance of different receivers for a 64-QAM OFDM system with $N = 512$ and $O_s = 4$. The ADC is parameterized with $R_{bit} = 3$ bits of resolution and variable saturation levels.

From the figure, it can be noted that the presence of the imperfect ADC significantly degrades the detection performance of the conventional ZF receiver, regardless of the considered A_{sat}. For $A_{sat} = 8\sigma^2$, where $\sigma^2 = \text{var}[X_k]/2$, the ZF presents a high BER floor. For a target BER of 10^{-4}, the performance loss of the GAMP and Bussgang receivers relatively to the ideal receiver is approximately 13 dB. For $A_{sat} = 4\sigma^2$, the nonlinear distortion due to signal clipping is larger, while the quantization noise for the signal below A_{sat} is reduced, compared to the previous case. The Bussgang and GAMP receivers take advantage of this fact to improve performance, reaching a target BER of 10^{-4} at 9 dB of E_b/N_0 from the ideal receiver, i.e., a 4 dB reduction over using a larger A_{sat}. The similar performance of both receivers indicates that the nonlinear distortion present in the signal is being successfully mitigated.

Fig. 3 presents the BER results with $R_{bit} = 4$. From the figure, it is interesting to note how a single bit drastically affects the performance of all receivers. When $A_{sat} = 8\sigma^2$, the ZF receiver achieves a BER floor close to 10e-4, while the Bussgang and GAMP receivers significantly outperform it, achieving the target BER of 10e-4 at an additional 5 dB of E_b/N_0, compared to the linear case. For $A_{sat} = 4\sigma^2$, the conventional receiver cannot recover the signal at all, whereas Bussgang and GAMP perform only 3 dB worse than the ideal receiver. In this situation, there is no clear advantage to using GAMP over Bussgang, however, this is not the case for higher-order modulation. Fig. 4 shows the BER performance for 256-QAM with $R_{bit} = 4$. For a larger constellation, we have increased the bit resolution to $R_{bit} = 4$, without changing the remaining parameters. When $A_{sat} = 8\sigma^2$, the Bussgang and GAMP receivers can achieve a target BER of 10^{-4} at the cost of approximately 12 dB in E_b/N_0. However, for the lower saturation value $A_{sat} = 4\sigma^2$, Bussgang receiver does not reach the target BER, while GAMP can achieve the target, while requiring only 6 more dB of E_b/N_0 than the ideal receiver,

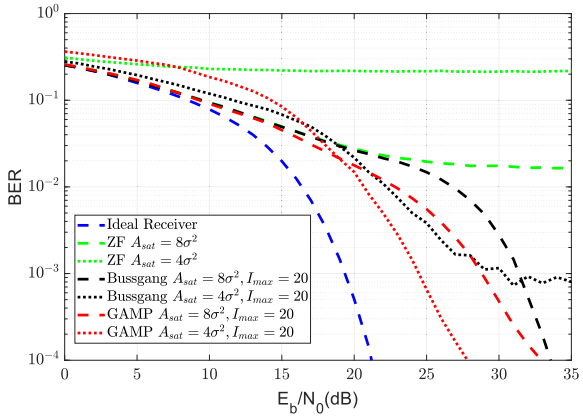

FIGURE 4. BER as a function of the E_b/N_0, for 256-QAM with $R_{bit} = 4$, compared with a conventional ZF, Bussgang receiver, and GAMP with $N_x = 1024$.

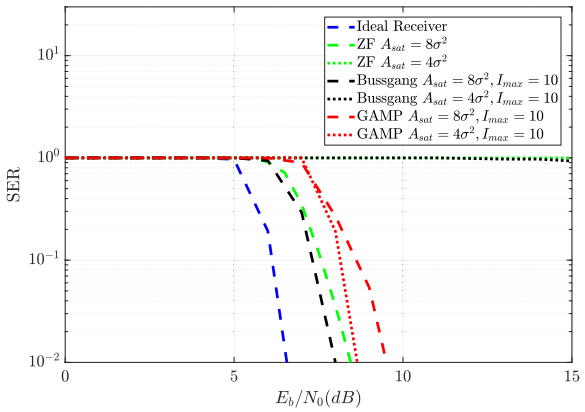

FIGURE 5. SER as a function of the E_b/N_0, for 64-QAM with $R_{bit} = 3$, for Bussgang and GAMP receivers with $N_x = 64$ and $\beta = 0.85$.

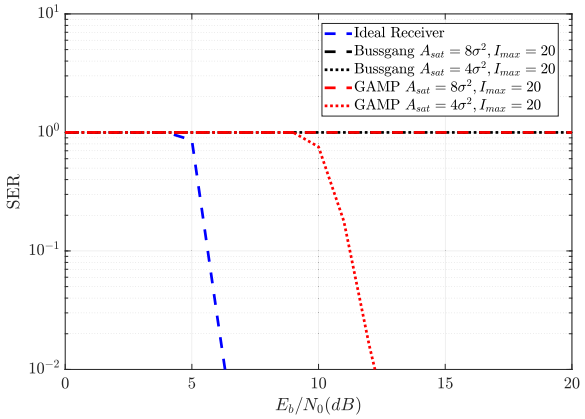

FIGURE 6. SER as a function of the E_b/N_0, for 64-QAM with $R_{bit} = 2$, for Bussgang and GAMP receivers with $N_x = 64$ and $\beta = 0.85$.

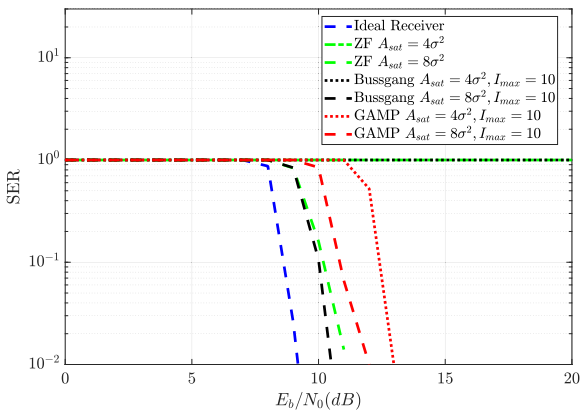

FIGURE 7. SER as a function of the E_b/N_0, for 256-QAM with $R_{bit} = 4$, for Bussgang and GAMP receivers with $N_x = 256$ and $\beta = 0.85$.

making this receiver a more effective option for this scenario. The poor performance of Bussgang is due to its limited distortion cancellation performance for large constellations, as it relies on estimating the transmitted signal. Comparing with Fig. 3, GAMP enables a receiver with an ADC resolution of $N_{bits} = 4$ to support 256-QAM, at the cost of approximately 6 dB in E_b/N_0 from an ideal 256-QAM system.

B. FREQUENCY-SELECTIVE CHANNELS WITH PERFECT CSI

For the following results, we consider a highly frequency-selective channel where the channel frequency responses H_k are modeled by a complex random variable. This channel is randomized for each OFDM block transmission. We also consider A $R = 1/2$ rate LDPC code with $N_P = 2016$ and $K_P = 1008$ is used to cope with the selective channel [26], where coded bits are interleaved randomly within each OFDM symbol. Due to the code gain of the LDPC, the GAMP damping parameter was increased to $\beta = 0.85$, and N_x was set to 64 and 256 for 64-QAM and 256-QAM, respectively. The symbol error rate (SER), which is defined as the probability that an OFDM symbol has at least 1 incorrect bit, is selected as the performance metric. This metric is commonly used to compare performance when block-based FEC is employed, due to the error propagation that can occur when a block cannot be decoded. As such, this metric is a better measure of the actual performance. For these simulations, a target SER of 10^{-2} was chosen. For the results in this section, we utilized a larger number of subcarriers, $N = 1024$.

Fig. 5 presents the SER of different reception schemes considering an ADC with $R_{bit} = 3$ bits of resolution.

As can be observed from the figure, the addition of channel coding allows the conventional receiver to perform adequately even for $R_{bit} = 3$. In this case, the code gain is sufficient to compensate for the nonlinearity, except in the case of low A_{sat}, where only GAMP can achieve an acceptable SER.

In Fig. 6 is presented the SER considering $R_{bit} = 2$.

From the figure, the GAMP performance benefits are clear, since the GAMP receiver presents a much better performance than the Bussgang receiver. The ZF receiver was omitted due to its SER being 1 for all E_b/N_0 in this scenario. For $A_{sat} = 4\sigma^2$, only the GAMP receiver achieves the target SER of 10^{-2} at an E_b/N_0 of 12 dB, which is a loss of only 6 dB relatively to the ideal receiver. For $A_{sat} = 8\sigma^2$, neither receiver can achieve an SER lower than 1 due to the higher quantization noise.

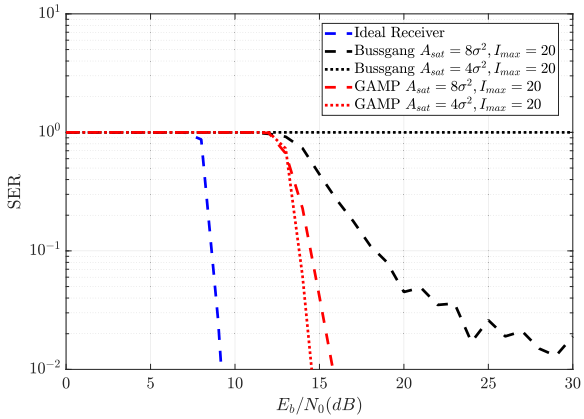

FIGURE 8. SER as a function of the E_b/N_0, for 256-QAM with $R_{bit} = 3$, compared with a Bussgang receiver, and GAMP with $N_x = 256$ and $\beta = 0.85$.

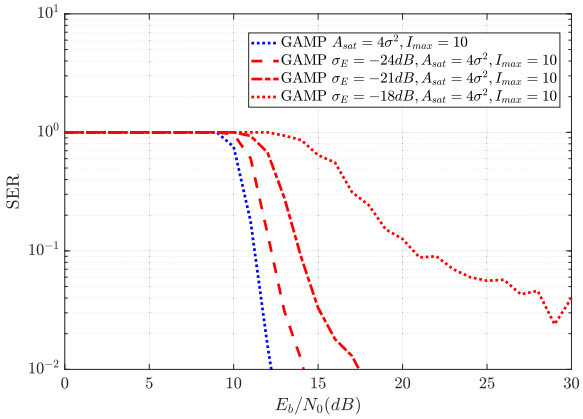

FIGURE 9. SER as a function of the E_b/N_0, for imperfect CSI 64-QAM with $R_{bit} = 2$ of GAMP with $N_x = 64$ and $\beta = 0.85$.

TABLE 2. Comparison of the Median Number of Iterations Required for Convergence, Considering Different System Configurations

System parameters	Median Number of Iterations
64-QAM@25dB $O_s = 4$	9
LDPC 64-QAM@15dB $O_s = 4$	4
256-QAM@28dB $O_s = 4$	14
LDPC 256-QAM@17dB $O_s = 4$	6

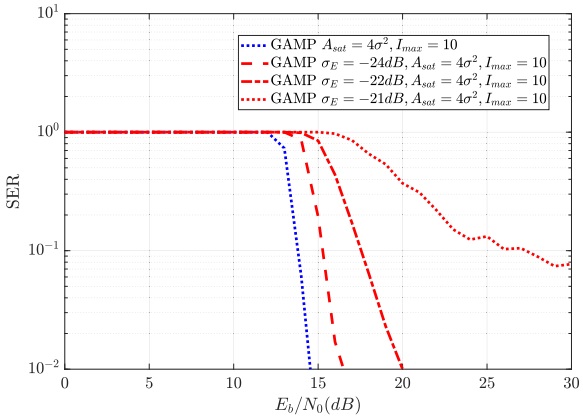

FIGURE 10. SER as a function of the E_b/N_0, for imperfect CSI 256-QAM with $R_{bit} = 3$, of GAMP with $N_x = 256$ and $\beta = 0.85$.

Fig. 7 presents the SER for a 256-QAM system, using $R_{bit} = 4$. As was the case for 64-QAM, the coding gain allows the conventional receiver to perform well with only $R_b = 4$ bits of ADC resolution. The GAMP receiver can recover the signal even for low A_{sat}, though it performs worse for higher A_{sat}.

Fig. 8 shows the SER considering $R_{bit} = 3$.

The performance of the ZF receiver was omitted for clarity, as the SER was 1 for all E_b/N_0. In the uncoded case, it was necessary to increase the ADC resolution to maintain performance. With the LDPC, however, Bussgang shows a modest improvement, though it cannot reach an SER below 10^{-2}. The GAMP receiver can achieve a much better performance, reaching the target SER of 10^{-2} at only 5 and 6 dB of E_b/N_0 from the linear receiver, with $A_{sat} = 4\sigma^2$ and $A_{sat} = 8\sigma^2$. As was seen in previous results, GAMP performs better when the saturation value is lower due to the increased clipping. It should be highlighted that this is the same ADC resolution as shown in Fig. 5, which demonstrates how GAMP can support 256-QAM even when the ADC was selected for 64-QAM.

An additional benefit of combining the LDPC decoding within GAMP iterations is the reduced number of iterations necessary for convergence. Table 2 compares the median number of iterations for both receivers considering the various simulated scenarios.

The addition of LDPC decoding can reduce the necessary iterations by up to 56%, greatly reducing the total complexity of iterative GAMP over uncoded implementations.

C. FREQUENCY-SELECTIVE CHANNELS WITH IMPERFECT CSI

In this section, we consider the impact of imperfect CSI on the proposed receiver. We consider the coded scenarios from the previous section. The CSI error is represented by the variance σ_E, which was defined in (24). In fig. 9 we present the SER of 64-QAM for $R_{bit} = 2$ and imperfect CSI.

From the figure, we observe that for $\sigma_E = -24$ dB, GAMP's performance is only about 1.5 dB worse than the ideal CSI scenario. For $\sigma_E = -21$ dB, results in a performance degradation of approximately 4 dB, assuming a target SER of 10^{-2}. With $\sigma_E = -18$ dB, the SER is significantly higher, and the target SER of 10^{-2} is not achieved within the simulated E_b/N_0 range. Fig. 10 shows the SER for 256-QAM with $R_{bit} = 3$ and imperfect CSI.

From the figure, it can be observed that a higher-order constellation shows a higher sensitivity to CSI errors. For $\sigma_E = -24$ dB, there is a slight degradation of approximately 1.5 dB in E_b/N_0 for the target SER 10^{-2}. At $\sigma_E = -22$ dB,

the degradation is significantly high, at approximately 5 dB of E_b/N_0, for the same target. For CSI error variances $\sigma_E \geq -21$ dB, the receiver does not reach the target SER.

VII. CONCLUSION

In this work, a GAMP receiver that is usually designed to cope with transmitter-side nonlinearities was employed to handle receiver-side nonlinearities. It was shown that GAMP can be used to support high-order constellations even when the resolution of the ADC is low. This is explained by the fact that GAMP can take advantage of the nonlinear distortion associated with the clipping effects of the ADC. In the presence of channel fading, the proposed LDPC coded GAMP receiver was able to mitigate the distortion from the ADC, even in the presence of channel estimation errors. As such, the GAMP receiver can be an interesting option for improving detection and supporting high-order QAM when using low-resolution ADCs.

REFERENCES

[1] B. Murmann, "The race for the extra decibel: A brief review of current ADC performance trajectories," *IEEE Solid-State Circuits Mag.*, vol. 7, no. 3, pp. 58–66, Summer 2015.

[2] R. H. Walden, "Analog-to-digital converter survey and analysis," *IEEE J. Sel. Areas Commun.*, vol. 17, no. 4, pp. 539–550, Apr. 1999.

[3] J. Liu, Z. Luo, and X. Xiong, "Low-resolution ADCs for wireless communication: A comprehensive survey," *IEEE Access*, vol. 7, pp. 91291–91324, 2019.

[4] J. Guerreiro, R. Dinis, and P. Montezuma, "Low-complexity SC-FDE techniques for massive MIMO schemes with low-resolution ADCs," *IEEE Trans. Commun.*, vol. 67, no. 3, pp. 2368–2380, Mar. 2019.

[5] C. K. Sheemar and D. Slock, "Receiver design and AGC optimization with self interference induced saturation," in *Proc. IEEE Int. Conf. Acoust., Speech Signal Process.*, 2020, pp. 5595–5599.

[6] J. Bussgang, "Crosscorrelation functions of amplitude-distorted gaussian signals," Massachusetts Inst. Technol. Res. Lab. Electron., Tech. Rep. 216, Mar. 1952.

[7] J. Guerreiro, R. Dinis, P. Montezuma, and M. Campos, "On the receiver design for nonlinear NOMA-OFDM systems," in *Proc. IEEE 91st Veh. Technol. Conf.*, 2020, pp. 1–6.

[8] S. Rangan, P. Schniter, A. K. Fletcher, and S. Sarkar, "On the convergence of approximate message passing with arbitrary matrices," *IEEE Trans. Inf. Theory*, vol. 65, no. 9, pp. 5339–5351, Sep. 2019.

[9] S. V. Zhidkov, "Orthogonal transform multiplexing with memoryless nonlinearity: A possible alternative to traditional coded-modulation schemes," in *Proc. IEEE 9th Int. Congr. Ultra Modern Telecommun. Control Syst. Workshops*, 2017, pp. 209–214.

[10] S. Zhidkov and R. Dinis, "Belief propagation receivers for near-optimal detection of nonlinearly distorted OFDM signals," in *Proc. IEEE 89th Veh. Technol. Conf.*, 2019, pp. 1–6.

[11] M. J. L. Morales, R. Dinis, and A. G. Armada, "Near-optimal detection of CE-OFDM signals with high power efficiency via GAMP-based receivers," in *Proc. IEEE Globecom Workshops*, 2022, pp. 7–12.

[12] C. Yang, X. Liu, Y. L. Guan, and R. Liu, "Fast GAMP algorithm for nonlinearly distorted OFDM signals," *IEEE Commun. Lett.*, vol. 25, no. 5, pp. 1682–1686, May 2021.

[13] T. M. Cover and J. A. Thomas, *Elements of Information Theory*, 2nd ed. Hoboken, NJ, USA: Wiley, 2012.

[14] Y. Xiong, N. Wei, and Z. Zhang, "A low-complexity iterative GAMP-based detection for massive MIMO with low-resolution ADCs," in *Proc. IEEE Wireless Commun. Netw. Conf.*, 2017, pp. 1–6.

[15] C. Cao, H. Li, and Z. Hu, "An AMP based decoder for massive MU-MIMO-OFDM with low-resolution ADCs," in *Proc. IEEE Int. Conf. Comput. Netw. Commun.*, 2017, pp. 449–453.

[16] H. Wang, W. T. Shih, C. K. Wen, and S. Jin, "Reliable OFDM receiver with ultra-low resolution ADC," *IEEE Trans. Commun.*, vol. 67, no. 5, pp. 3566–3579, May 2019.

[17] S. Jacobsson, G. Durisi, M. Coldrey, and C. Studer, "Linear precoding with low-resolution DACs for massive MU-MIMO-OFDM downlink," *IEEE Trans. Commun.*, vol. 18, no. 3, pp. 1595–1609, Mar. 2019.

[18] E. Balevi and J. G. Andrews, "One-bit OFDM receivers via deep learning," *IEEE Trans. Commun.*, vol. 67, no. 6, pp. 4326–4336, Jun. 2019.

[19] X. Song, S. Ma, P. Neuhaus, W. Wang, X. Gao, and G. Fettweis, "On robust millimeter wave line-of-sight MIMO communications with few-bit ADCs," *IEEE Trans. Commun.*, vol. 21, no. 12, pp. 11164–11178, Dec. 2022.

[20] P. Arpaia, P. Daponte, and L. Michaeli, "Influence of the architecture on ADC error modeling," *IEEE Trans. Instrum. Meas.*, vol. 48, no. 5, pp. 956–966, Oct. 1999.

[21] R. M. Gray, "Quantization noise spectra," *IEEE Trans. Inf. Theory*, vol. 36, no. 6, pp. 1220–1244, Nov. 1990.

[22] J. Guerreiro, R. Dinis, and P. Montezuma, "Optimum and sub-optimum receivers for OFDM signals with strong nonlinear distortion effects," *IEEE Trans. Commun.*, vol. 61, no. 9, pp. 3830–3840, Sep. 2013.

[23] X. Cheng, B. Xia, K. Xu, and S. Li, "Bayesian channel estimation and data detection in oversampled OFDM receiver with low-resolution ADC," *IEEE Trans. Wireless Commun.*, vol. 9, no. 20, pp. 5558–5571, Sep. 2021.

[24] R. W. Stewart and E. Pfann, "Oversampling and sigma-delta strategies for data conversion," *Electron. Commun. Eng. J.*, vol. 10, no. 1, pp. 37–47, 1998.

[25] "5G; NR; Physical channels and modulation," Version 17.4.0, 3rd Generation Partnership Project (3GPP),2023 .

[26] *IEEE Standard for Air Interface for Broadband Wireless Access Systems*, IEEE Standard 802.16-2017 (Revision of IEEE Standard 802.16-2012), 2018.

[27] J. Mo, P. Schniter, N. G. Prelcic, and R. W. Heath, "Channel estimation in millimeter wave MIMO systems with one-bit quantization," in *Proc. IEEE 48th Asilomar Conf. Signals Syst. Comput.*, 2014, pp. 957–961.

[28] Q. Zou, H. Zhang, D. Cai, and H. Yang, "Message passing based joint channel and user activity estimation for uplink grant-free massive MIMO systems with low-precision ADCs," *IEEE Signal Process. Lett.*, vol. 27, pp. 506–510, 2020.

[29] M. Y. Takeda, A. Klautau, A. Mezghani, and R. W. Heath, "MIMO channel estimation with non-ideal ADCs: Deep learning versus GAMP," in *Proc. IEEE 29th Int. Workshop Mach. Learn. Signal Process.*, 2019, pp. 1–6.

[30] J. Guerreiro, R. Dinis, and P. Montezuma, "Analytical performance evaluation of precoding techniques for nonlinear massive MIMO systems with channel estimation errors," *IEEE Trans. Commun.*, vol. 66, no. 4, pp. 1440–1451, Dec. 2017.

[31] M. Tuchler, A. C. Singer, and R. Koetter, "Minimum mean squared error equalization using a priori information," *IEEE Trans. Inf. Theory*, vol. 50, no. 3, pp. 673–683, Mar. 2002.

[32] J. Madeira, J. Guerreiro, and R. Dinis, "Iterative frequency-domain detection and compensation of nonlinear distortion effects for MIMO systems," *Phys. Commun.*, vol. 37, 2019, Art. no. 100869.

[33] T. Cui, F. Gao, A. Nallanathan, H. Lin, and C. Tellambura, "Iterative demodulation and decoding algorithm for 3GPP/LTE-A MIMO-OFDM using distribution approximation," *IEEE Trans. Wireless Commun.*, vol. 17, no. 2, pp. 1331–1342, Feb. 2018.

JOÃO MADEIRA received the master's degree in electrical engineering and computer science from the Nova School of Science and Technology, Lisbon, Portugal, where he is currently working toward the Ph.D. degree. He has worked in R&D with technological startups in several European research projects involving UAVs and secure wireless communications. His mains research interests include high efficiency wireless transmission, software defined radios, and forward error correction.

ZAHRA MOKHTARI (Member, IEEE) received the B.Sc. degree in electrical engineering from the University of Yazd, Yazd, Iran, in 2011, and the M.Sc. and the Ph.D. degrees in electrical engineering from the University of Tehran, Tehran, Iran, in 2013 and 2019, respectively. In 2017, she was a Visiting Researcher with the Chalmers University of Technology, Gothenburg, Sweden. From 2018 to 2022, she was a Researcher with Science and Technology Park, Yazd. Since 2022, she has been a Researcher with the Instituto de Telecomunicações, Lisbon, Portugal. Her research interests include wireless communications, 5G, cell free and cellular massive MIMO, and hardware impairments.

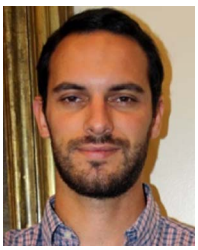

JOÃO GUERREIRO (Senior Member, IEEE) received the M.Sc. and Ph.D. degrees in electrical and computer engineering from the Faculdade de Ciências e Tecnologias da Universidade Nova de Lisboa, Lisbon, Portugal, in 2012 and 2016, respectively. Since 2013, he has been actively involved in scientific research in the field of wireless communications, including signal processing, transceiver design and channel modeling. He has authored or coauthored more than 25 journal articles, 50 conference articles (one best paper award), three patents (granted or pending) and one book chapter. He has participated in several national and international research projects in the last years. He is currently an Assistant Professor with Faculdade de Ciências e Tecnologias da Universidade Nova de Lisboa and a Researcher with Instituto de Telecomunicações. Since 2018, he has been one of the founders of Koala Tech.

RUI DINIS (Senior Member, IEEE) received the Ph.D. degree from Instituto Superior Técnico (IST), Technical University of Lisbon, Lisbon, Portugal, in 2001, and the Habilitation degree in telecommunications from Faculdade de Ciências e Tecnologia (FCT), Universidade Nova de Lisboa (UNL), Lisbon, in 2010. From 2001 to 2008, he was an Assistant Professor with IST. He is currently a Full Professor with FCT-UNL. In 2003, he was an invited Researcher with Carleton University, Ottawa, ON, Canada. He was a Researcher with Centro de Análise e Processamento de Sinal, IST, from 1992 to 2005, and a Researcher with Instituto de Sistemas e Robótica from 2005 to 2008. Since 2009, he has been a Senior Researcher with Instituto de Telecomunicações. His research interests include transmission, estimation, and detection techniques for wireless communications. He is a VTS Distinguished Speaker and ComSoc Distinguished Lecturer. He is or was the Editor of IEEE TRANSACTIONS ON WIRELESS COMMUNICATIONS, IEEE TRANSACTIONS ON COMMUNICATIONS, IEEE TRANSACTIONS ON VEHICULAR TECHNOLOGY, IEEE OPEN JOURNAL ON COMMUNICATIONS, and *Elsevier Physical Communication*. He was also a guest editor of several special issues.